

Article

The Role of Nickel and Brønsted Sites on Ethylene Oligomerization with Ni-H-Beta Catalysts

Gabriel V. S. Seufitelli ^{1,*}, Jason J. W. Park ¹, Phuong N. Tran ¹, Anthony Dichiara ¹, Fernando L. P. Resende ² and Rick Gustafson ¹

¹ School of Environmental and Forest Sciences, University of Washington, Seattle, WA 98195, USA; jjpark987@gmail.com (J.J.W.P.); trann1995@gmail.com (P.N.T.); abdichia@uw.edu (A.D.); pulp@uw.edu (R.G.)

² Jasper Department of Chemical Engineering, University of Texas at Tyler, Tyler, TX 75799, USA; fresende@uttyler.edu

* Correspondence: vianasg@uw.edu

Abstract: The present work studies the adsorption of ethylene on Ni-H-Beta particles to unravel the roles of nickel and Brønsted sites in the catalytic oligomerization of ethylene. Three models (i.e., two based on the Cossee–Arlman mechanism and one based on the metallacycle mechanism) are examined in terms of the nature of the active sites and the adsorption mechanism involved in the ethylene coordination step. The results are consistent with the participation of two active sites in the formation of $[\text{Ni}(\text{II})\text{-H}]^+$ Cossee–Arlman centers and also suggest that ethylene dissociates upon adsorption on $[\text{Ni}(\text{II})\text{-H}]^+$ sites. Further characterization of Ni-H-Beta catalysts prepared at different nickel loadings and silica-to-alumina ratios reveals that highly dispersed Ni^{2+} exists on the catalyst surface and interacts with the catalyst's lattice oxygen and free NiO crystals. At the same time, the kinetic results indicate that Brønsted sites may form isolated nickel-hydride ($[\text{Ni}(\text{II})\text{-H}]^+$) centers on the catalyst surface. In addition, the presence of residual, noncoordinated Ni^{2+} and Brønsted sites (not involved in the formation of $[\text{Ni}(\text{II})\text{-H}]^+$ sites) shows a reduced probability of the formation of nickel-hydride sites, hindering the conversion rate of ethylene. A mechanism for forming $[\text{Ni}(\text{II})\text{-H}]^+$ centers is proposed, involving ethylene adsorption over Ni^{2+} and a Brønsted site. This research has important implications for improving ethylene oligomerization processes over nickel-based heterogeneous catalysts.

Keywords: ethylene oligomerization; nickel-based heterogeneous catalyst; Brønsted acid sites; adsorption; Langmuir isotherms; Cossee–Arlman mechanism



Citation: Seufitelli, G.V.S.; Park, J.J.W.; Tran, P.N.; Dichiara, A.; Resende, F.L.P.; Gustafson, R. The Role of Nickel and Brønsted Sites on Ethylene Oligomerization with Ni-H-Beta Catalysts. *Catalysts* **2022**, *12*, 565. <https://doi.org/10.3390/catal12050565>

Academic Editor: Jason C. Hicks

Received: 5 May 2022

Accepted: 18 May 2022

Published: 20 May 2022

Publisher's Note: MDPI stays neutral with regard to jurisdictional claims in published maps and institutional affiliations.



Copyright: © 2022 by the authors. Licensee MDPI, Basel, Switzerland. This article is an open access article distributed under the terms and conditions of the Creative Commons Attribution (CC BY) license (<https://creativecommons.org/licenses/by/4.0/>).

1. Introduction

Ethylene oligomerization is a chemical process of foremost importance in producing higher alkenes, which are feedstocks for a wide range of fuels and chemicals. Currently, the oligomerization of ethylene is performed commercially with homogeneous catalysts [1–4]. Even though these catalysts are effective, they do not follow green chemistry principles due to the use of co-catalysts, such as methyl aluminoxane (MAO) or AlEtCl_2 , in excess that are usually dissolved in organic solvents such as toluene [2,3,5–7]. Also, homogeneous catalytic processes require expensive equipment to separate the catalyst from the products in the reactor effluent [2,8–10]. Because of this, there has been a significant effort to develop heterogeneous catalysts capable of oligomerizing ethylene at high conversions since these catalysts do not require the use of solvents, can be easily recovered and regenerated, and are more environmentally friendly than their homogeneous counterparts [2,8,11].

Several studies have proposed heterogeneous catalysts for ethylene oligomerization [4,6,11–23]. These reports have focused on introducing metals on acidic aluminosilicate supports (i.e., nickel-exchanged zeolites) to simulate the catalytic system employed

in homogeneous oligomerization processes. Among the proposed heterogeneous catalysts, Ni-H-Beta is an outstanding option for producing higher alkenes under mild conditions [4,9,11,19,24–27]. Martinez et al. were the first to report the production of liquid products using Ni-H-Beta catalysts, achieving conversions as high as 87% at 120 °C and 35 bar [11]. In recent publications from our group, we have reported the production of liquid products during ethylene oligomerization with Ni-H-Beta under a wide range of conditions [24–27].

The mechanism of ethylene oligomerization with nickel-based solid catalysts has been the focus of recent publications [5,28–32]. Joshi et al. summarized these recent findings in a review published in 2020 [33]. These reports agree that the mechanism of ethylene oligomerization with heterogeneous catalysts is similar to those observed in homogeneous catalytic systems. The most accepted mechanisms for ethylene oligomerization with nickel-based heterogeneous catalysts are shown in Figure 1.

Mechanisms A and B (Figure 1), denoted as Cossee–Arlman [34,35], involve the formation of nickel-hydride ($[\text{Ni}(\text{II})\text{-H}]^+$) Cossee–Arlman sites. The mechanism involved in the formation of the nickel-hydride Cossee–Arlman sites is controversial. Moussa et al. [5] recently proposed that ethylene dissociates over Ni^{2+} sites, forming a nickel-hydride Cossee–Arlman center—similar to the mechanism depicted in Figure 1 **Mechanism A**—where both the ethenyl and hydride species remain adsorbed on the same nickel site [33]. Conversely, Joshi et al. proposed that these sites are formed during an induction period (a short period before the formation of alkene products, usually at the onset of the reaction), and their formation rates are affected by the reaction conditions (pretreatment conditions, ethylene pressure, and reactor temperature) [5,33]. As noted by Joshi et al., the mechanism proposed by Moussa et al. combines the “in situ” formation of nickel-hydride with the adsorption of ethylene on the nickel site involving a +2/+4 redox cycle, contradicting previous X-ray adsorption studies [31,36] that have indicated the formation of the hydride species before ethylene adsorption on the catalyst (a “self-activation” mechanism via metal–ligand reaction), in which nickel has a +2 oxidation state. Another hypothesis for the formation of nickel-hydride sites involves the participation of Brønsted sites. Based on a spectroscopy study, Brückner et al. showed that Brønsted sites act as precursors in the “in situ” formation of $[\text{Ni}(\text{II})\text{-H}]^+$ intermediates via the oxidative addition of Brønsted sites to Ni^0 during the dimerization of butene with nickel-exchanged acidic catalysts [37]. The same mechanism was investigated later by Brogaard and Olsbye via DFT calculations for ethylene oligomerization with nickel-based heterogeneous catalysts [28]. The oxidation of metallic nickel occurs during an induction period and can form either $[\text{Ni}(\text{I})\text{-H}]$ or $[\text{Ni}(\text{II})\text{-H}]^+$ [37]. Ng et al. proposed a similar mechanism involving the combination of Ni^+ and H^+ to produce a $[\text{Ni}(\text{I})\text{-H}(\text{I})]^{2+}$ site during the dimerization of ethylene over Ni-Y catalysts [38]. It is worth mentioning that a recent study showed that $[\text{Ni}(\text{II})\text{-H}]^+$ sites can form in the absence of residual Brønsted sites [31], but this does not necessarily rule out the participation of H^+ in the formation of these sites. Indeed, according to Moussa et al. [5], a proton is formed upon ethylene dissociation over nickel zeolites, and the proton combines with the nickel site (Ni^{2+}) to produce an $[\text{ethenyl-Ni}(\text{II})\text{-H}]^+$ intermediate. Although the mechanism involved in the active site formation for ethylene oligomerization remains controversial, these studies agree that, once nickel-hydride sites are formed, the catalytic cycle proceeds with ethylene coordination-insertion steps over the $[\text{Ni}(\text{II})\text{-H}]^+$ sites, forming $[\text{ethene-Ni}(\text{II})\text{-alkyl}]^+$ intermediates followed by β -hydride elimination to form alkene products (i.e., butene, hexene, and octene). Our group recently published a detailed microkinetic model based on the Cossee–Arlman mechanism described above (similar to the mechanism shown in Figure 1 **Mechanism B**) for ethylene oligomerization with a Ni-H-Beta catalyst [39].

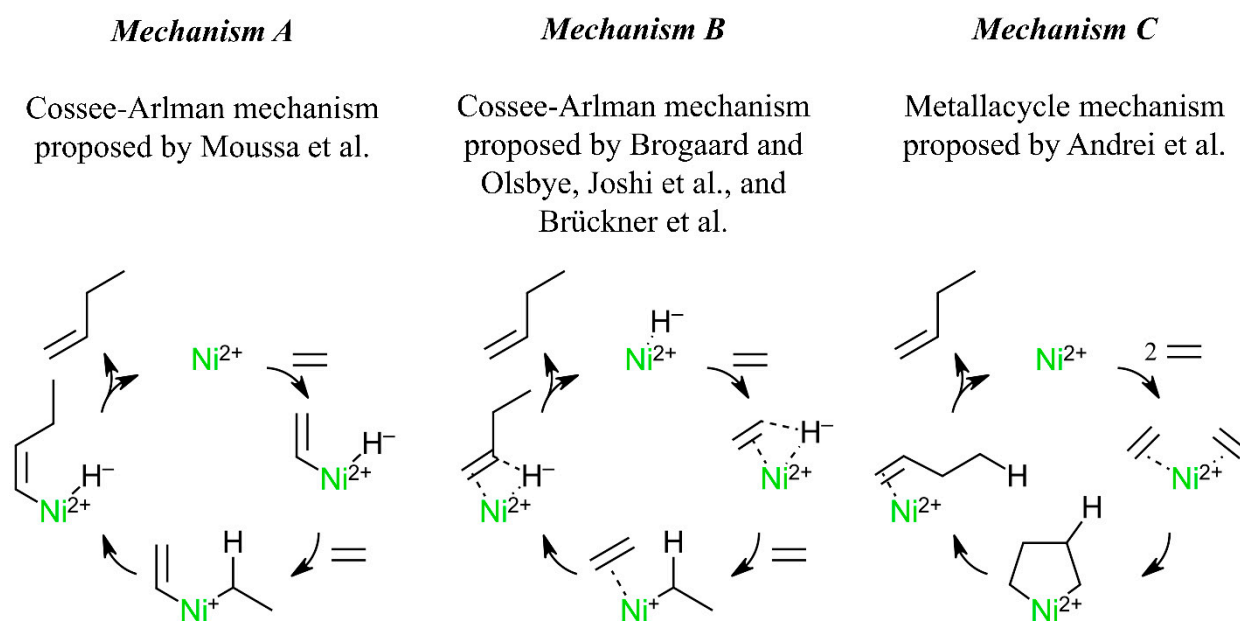


Figure 1. Simplified reaction mechanisms proposed in the literature (adapted from Moussa et al. [5], Brogaard and Olsbye et al. [28], Brückner et al. [37], and Joshi et al. [31,33]) for ethylene oligomerization over nickel-based solid catalysts. *Mechanisms A* and *B* are based on the Cossee–Arlman mechanism, and *Mechanism C* is based on the metallacycle mechanism.

Mechanism C, denoted as metallacycle, involves coupling two ethylene molecules over a cationic center (i.e., Ni^{2+}), forming a metallacycle pentane species. Further insertion of ethylene leads to an increase in the carbon number of the metallacycle species, which eventually desorbs as an alkene. Andrei et al. proposed that a metallacycle mechanism was involved in ethylene oligomerization over Ni-ALSBA-15. The authors postulated this mechanism based on the absence of a co-catalyst or “in situ” activation step before the reaction; a co-catalyst is not required to form the active center in the metallacycle mechanism [6]. It is important to note that some nickel catalysts promote oligomerization or polymerization reactions without an external co-catalyst, as explained previously [40,41]. Also, the metallacycle mechanism only leads to terminal alkene dimers [3], while the coordination-insertion mechanism leads to internal and terminal alkene dimers [42]. Internal alkenes are usually present among the products of ethylene oligomerization with heterogeneous nickel-based aluminosilicate catalysts (e.g., Ni-H-Beta).

Mechanisms B and *C* depicted in Figure 1 were investigated via DFT calculations by Brogaard and Olsbye. According to the authors, the most plausible mechanism for ethylene oligomerization over Ni-SSZ-24 catalysts [28] involved the formation of $[\text{Ni}(\text{II})\text{-H}]^+$ Cossee–Arlman active centers from the adsorption of ethylene over isolated Ni^{2+} (Figure 1—*Mechanism B*). More recently, Brogaard et al. [32] proposed via DFT calculations that Ni^{2+} in exchanging positions acts as a mobile active center, where the coordination of ethylene molecules triggers the reversible mobilization of these centers. Additional publications have postulated isolated Ni^+ and $[\text{Ni}(\text{II})\text{-OH}]^+$ species as the active sites involved in ethylene oligomerization over nickel-exchanged solid catalysts [13,23,28,43–46]. Based on the main investigations reported in the literature, Ni^+ , Ni^{2+} , $[\text{Ni}(\text{I})\text{-H}]$, $[\text{Ni}(\text{II})\text{-H}]^+$, and $[\text{Ni}(\text{II})\text{-OH}]^+$ sites have been proposed as active sites during the conversion of ethylene into alkenes over nickel-based heterogeneous catalysts. According to Brogaard and Olsbye, it is unclear if $[\text{Ni}(\text{II})\text{-OH}]^+$ species are likely to survive the elevated catalyst pretreatment temperatures [28], and Joshi et al. indicated that experimental evidence supporting the formation of ethanol, ethanal, or 1,3-butadiene (reaction byproducts for the proposed mechanism) during ethylene oligomerization over $[\text{Ni}(\text{II})\text{-OH}]^+$ sites is not well-supported in the literature [33]. However, Agirrezabal-Telleria and Iglesia [46] provided strong

evidence that $[\text{Ni}(\text{II})\text{-OH}]^+$ species are the active sites during ethylene oligomerization over NiAl-MCM-41 catalysts, where the authors showed that the suppression of both Ni^{2+} and H^+ sites led to a decrease in oligomerization rates, even at a high reaction temperature of 448 K.

The studies reported by Brückner et al. [37] and Ng et al. [38] are among the few that have postulated the participation of Brønsted sites during the “in situ” formation of nickel-hydride active centers. Also, DFT calculations and experimental studies have suggested that additional Brønsted sites may form during ethylene coordination with nickel sites, increasing catalyst acidity [5,28,47]. These may participate in oligomerization reactions involving ethylene or higher alkenes products. It has been shown in the literature that the extent of ethylene oligomerization over Brønsted sites at mild conditions is small or negligible [48]. Nonetheless, it is plausible that there is a synergistic effect at mild conditions between nickel and Brønsted sites, as proposed by Brückner et al. [37] and Ng et al. [38]. According to DFT calculations, $[\text{Ni}(\text{II})\text{-H}]^+$ formed spontaneously when nickel and residual Brønsted sites were located close to each other [28]. Also, according to Forget et al., a single Brønsted site close to a nickel site is required to form the active site for ethylene oligomerization [29]. Chen et al. provided indications that catalysts with more uniform nickel spatial distribution and closer proximity between nickel and Brønsted sites exhibit higher chain-growth rates [49]. In a review from 2021 [50], E. Koninckx et al. pointed out that catalyst acidity is usually a topic of interest in heterogeneous catalytic systems that employ bifunctional catalysts, for instance, hydrocracking. The authors also stated that only a few studies have been devoted to unraveling the role of catalyst acidity during ethylene oligomerization with nickel-based heterogeneous catalysts.

The present study is part of a broader research effort to elucidate the mechanism and kinetics of ethylene oligomerization over nickel-based heterogeneous catalysts. The study reported in the present publication attempts to describe the role of nickel and Brønsted sites in ethylene oligomerization. We used a Ni-H-Beta catalyst because of its high activity in converting ethylene into higher alkenes and the large number of reports available in the literature for this catalyst. Initially, we present a comprehensive ethylene adsorption study. Even though previous studies have investigated ethylene adsorption on Ni-H-Beta via spectroscopy [4,5], this is the first work to report ethylene adsorption isotherms over this catalyst. Then, we perform extensive characterization of Ni-H-Beta catalysts with varying nickel loadings and silica-to-alumina ratios via X-ray photoelectron spectroscopy (XPS), X-ray powder diffraction (XRD), and pyridine adsorption. We also report new kinetic data for Ni-H-Beta catalysts. The adsorption study, catalyst characterization, and kinetic data obtained in the present work are used to compare different ethylene adsorption mechanisms, including the ones proposed in the literature (mechanisms depicted in Figure 1), specifically, the nature of the active site and the mechanism involved in the initial step of ethylene oligomerization over the Ni-H-Beta catalysts.

2. Experimental Method

2.1. Catalyst Synthesis

Ammonium-exchanged Beta zeolites with silica-to-alumina ratios ($\text{SiO}_2/\text{Al}_2\text{O}_3$) of 25 (product number = CP814E) and 39 (product number = CP814C) and the protonated form of the Beta zeolite with a $\text{SiO}_2/\text{Al}_2\text{O}_3$ ratio of 300 (product number = CP811-300) were purchased from Zeolyst International. Five Ni-H-Beta catalysts were produced by incipient wetness impregnation of the ammonium form of the Beta zeolite ($\text{SiO}_2/\text{Al}_2\text{O}_3 = 25$) with 0.07, 0.13, 0.25, 0.51, and 1.03 M solutions of $\text{Ni}(\text{NO}_3)_2$ purchased from Sigma-Aldrich (Purity: 99.999%, product number = 203874). This process produced Ni-H-Beta catalysts with nickel loadings of 1.0, 1.5, 2.5, 4.1, and 6.0 wt. % (as measured by inductively coupled plasma-atomic emission spectroscopy). Nickel catalysts (nickel loading = 2.5 wt. %) with different $\text{SiO}_2/\text{Al}_2\text{O}_3$ ratios were produced by incipient wetness impregnation of the ammonium ($\text{SiO}_2/\text{Al}_2\text{O}_3 = 39$) and protonated ($\text{SiO}_2/\text{Al}_2\text{O}_3 = 300$) forms of the Beta zeolite. The procedure used for producing nickel catalysts is described in previous publications

from our group [24–27,39]. Briefly, it involved the dropwise addition of a $\text{Ni}(\text{NO}_3)_2$ solution (100 mL total solution volume at a given $\text{Ni}(\text{NO}_3)_2$ concentration) onto 20 g of zeolite powder for 1 h, producing a slurry that was magnetically stirred for another 5 h using a Teflon stir bar. Then, the slurry was vacuum-filtered, followed by washing with deionized water. After filtration, the solids were dried at 100 °C overnight. After drying, a material resembling clay was obtained, which was ground using a mortar and pestle. Finally, the powder was calcined at 550 °C for 5 h to activate the catalyst.

Three additional H-Beta catalysts with $\text{SiO}_2/\text{Al}_2\text{O}_3$ ratios of 126, 146, and 216 ($\text{SiO}_2/\text{Al}_2\text{O}_3$ ratios were measured via X-ray fluorescence (XRF)) were produced by acidic treatment of the pristine H-Beta support ($\text{SiO}_2/\text{Al}_2\text{O}_3 = 39$) with 0.20, 0.40, and 0.60 M solutions of HNO_3 , respectively. The HNO_3 solution was mixed with the pristine support at 80 °C for 5 h under agitation. Then, the solution was vacuum-filtered, and the recovered solids were washed several times with deionized water until neutral pH was achieved, as determined by pH test strips. The filtered solids were dried overnight at 100 °C and calcined at 550 °C for 5 h to obtain the H-Beta catalysts with different $\text{SiO}_2/\text{Al}_2\text{O}_3$ ratios. After acidic treatment, the Ni-H-Beta catalysts were produced via incipient wetness impregnation, according to the procedure described previously.

2.2. Catalyst Characterization

2.2.1. Inductively Coupled Plasma-Atomic Emission Spectroscopy (ICP-AES)

ICP-AES was used to measure the nickel loadings of the catalysts according to EPA protocol 200.7. The catalyst samples were digested with nitric acid and hydrochloric acid prior to the ICP-AES measurements.

2.2.2. Pyridine Adsorption

Pyridine was purchased from TCI (purity > 99.0%, product number = Q0034). The adsorption experiments were conducted in a Harrick Sci. diffuse reflectance chamber mounted with ZnSe windows. The spectra were collected using a Shimadzu Prestige-21 Infrared Spectrophotometer equipped with a DLaTGS detector. The catalyst samples (5 mg diluted in KBr at 5% dilution) were pretreated at 300 °C under a vacuum (10^{-3} bar) for 30 min before sorption. After pretreatment, the temperature was reduced to 30 °C, and 20 μL of pyridine was introduced into the chamber under vacuum. The chamber was evacuated for 30 min to remove physisorbed pyridine species from the catalyst surface, and the reactor chamber temperature was increased to 250 °C. The spectrum of each catalyst surface was collected with a resolution of 8 cm^{-1} . Peaks located at 1450 and 1545 cm^{-1} were used to estimate the concentration of Lewis and Brønsted acid sites, respectively, using the extinction coefficients reported by Emeis [51].

2.2.3. X-ray Photoelectron Spectroscopy (XPS)

X-ray photoelectron spectra were collected using a Surface Science Instrumental S-Probe spectrometer (Service Physics, Bend OR) with a monochromatized Al X-Ray source and a spot size of 800 \times 800 μm . The sample powders were pressed onto a piece of double-sided Scotch tape. The samples were set as insulators, and a charge neutralizer was used during the measurements. All binding energies were referenced to the C1s of C-C bonds at 285.0 eV for the high-resolution spectra.

2.2.4. X-ray Powder Diffraction (XRD)

X-ray powder diffractions were obtained using a Bruker D8 Discover Microfocus diffractometer mounted with an $\text{I}\mu\text{S}$ 2.0 microfocus X-ray source (Incoatec) using Cu K- α radiation and a Pilatus 3R 100K-A 2D detector. The samples were pressed flat onto a silicon wafer substrate before measurement.

2.3. Ethylene Adsorption Experiments

A fixed-bed reactor was used to study the adsorption of ethylene on the Ni-H-Beta catalyst with a 4.1 wt. % nickel loading. The experiments were conducted at cryogenic temperatures of -77 and -20 °C by cooling the adsorption system in a dry-ice bath and a bath consisting of a mixture of ice and salt, respectively, to eliminate the extent of oligomerization reactions during the adsorption study. The temperature of the adsorption apparatus was kept approximately constant during each experiment with a variation of ± 0.5 °C. Before ethylene adsorption, 50 mg of fresh catalyst was packed inside the fixed bed (diameter = 0.5 cm and depth = 2.5 cm). Next, the catalyst was pretreated for 3 h at 300 °C under a nitrogen (Praxair, grade: 5.0, purity: 99.998%) flow of 100 mL/min to remove impurities and adsorbed water from the catalyst surface. Then, the adsorption system was cooled to the set-point temperature, and ethylene (Praxair, grade: 2.5, purity: 99.5%) was admitted into the fixed bed. Several experiments were performed at varying ethylene concentrations from 76 to 2100 ppm, and for each experiment, the ethylene concentration was kept constant. Gases at the outlet of the packed bed were analyzed using a GC-2014 (Shimadzu, Kyoto, Japan) equipped with a capillary column (Agilent 19091P-QO4 - ID = 0.32 mm, L = 30 m, and film = 20 μ m) and coupled with FID and TCD detectors. To minimize the gap between analyses, we ran the GC using an isothermal temperature of 40 °C for 5 min. After adsorption equilibrium was reached (determined from the uptake curves; not shown), the gases downstream of the reactor were analyzed using a different temperature profile (isothermal at 40 °C for 4 min, followed by heating to 130 °C at a rate of 30 °C/min and holding for 5 min, followed by heating to 260 °C at a rate of 10 °C/min and holding for 10 min) to verify whether products were generated during the adsorption. The spent catalysts were characterized after adsorption by FTIR (Shimadzu Prestige 21) to verify the presence of products on their surface. The FTIR spectra did not show peaks for C-H species on the catalysts after adsorption.

2.4. Ethylene Oligomerization Experiments

Ethylene oligomerization was carried out in a differential fixed-bed reactor, as described in our previous publication [39]. Briefly, 0.25 g of catalyst was loaded inside the fixed bed. Thermocouples at the center and on top of the catalyst bed were used to control the reactor temperature. A back-pressure regulator (ZF1 series, Equilibar) was used to control the reactor pressure, and the reactor outlet stream was mixed with nitrogen (Praxair, grade: 5.0, purity: 99.998%) for mass balance quantification. The gas mixture was fed into a GC-2014 (Shimadzu) equipped with an FID and a TCD detector coupled with a capillary column (Agilent 19091P-QO4 - ID = 0.32 mm, L = 30 m and film = 20 μ m).

Before ethylene oligomerization, the fresh catalyst was pretreated overnight (300 °C for 15 h) under a 100 mL/min nitrogen flow rate. After pretreatment, the temperature was reduced to the reaction temperature, and the reactor was pressurized to the reaction pressure with pure ethylene (Praxair, grade: 2.5, purity: 99.5%) at a flow rate of 700 mL/min to minimize the extent of the reaction at this point. After the reactor reached the reaction conditions, the ethylene flow rate was reduced from 700 mL/min to 160 mL/min, and we started the GC acquisition. Each experiment lasted at least 4 h until the system reached steady-state conditions. The mass balance closure for the experiments presented in this paper remained within $\pm 7\%$. The ethylene conversion was calculated according to Equation (1):

$$X = \frac{F_{products}}{F_{a0}} \quad (1)$$

where X is the ethylene conversion, F_{a0} is the ethylene mass feed rate ($\text{g}\cdot\text{min}^{-1}$), and $F_{products}$ is the mass flow rate of all products downstream of the reactor ($\text{g}\cdot\text{min}^{-1}$). The product selectivity was calculated according to Equation (2):

$$S_i \text{ (wt. \%)} = \frac{\text{mass of product } i}{\text{total mass of products}} \quad (2)$$

where S_i (wt. %) is the selectivity for species i in wt. %.

3. Results and Discussion

3.1. Ethylene Adsorption Study on Ni-H-Beta Catalyst

Adsorption isotherms can be obtained from sorption measurements of reactants or products (i.e., adsorbates) on the catalyst surface (i.e., adsorbent) under several adsorbate concentrations at a fixed temperature. Several adsorption isotherms have been developed for uniform and non-uniform surfaces. The Langmuir isotherm is used for uniform surfaces (ideal surfaces with the absence of attractive or repulsive molecular forces at the surface) and assumes the monolayer adsorption of molecules on a plain surface where all vacant sites are identical (constant surface enthalpy) [52,53]. For non-uniform surfaces (non-ideal or real surfaces with the presence of attractive or repulsive molecular forces at the surface), empirical isotherm models, such as Freundlich and Temkin, can be used to fit experimental adsorption data [53–55].

$$\frac{q}{q_0} = c' P^{\frac{1}{a}} \quad (3)$$

Equation (3) shows the Freundlich equation, where q/q_0 is the coverage (fraction of free sites occupied by molecules), P is the adsorbate pressure, and c' and a are adjusted constants that depend on temperature (c' also depends on the surface area of the adsorbent). Usually, c' and a decrease with temperature, and a positive value for the constant a is associated with repulsive molecular forces at the surface [56]. In addition to the empirical formulation, the Freundlich equation has been developed based on thermodynamic [57] and statistical [58–60] approaches assuming the adsorption of molecules on a heterogeneous surface divided into small domains containing similar sites [53]; an approach also proposed by Langmuir for heterogeneous surfaces [52].

The main difference between Langmuir and Freundlich isotherms is that the first assumes a uniform surface with equal affinities and energies, and the latter assumes a heterogeneous surface with sites having different affinities and energies. Also, while Langmuir isotherm expressions can be developed based on elementary adsorption steps of adsorbates on the catalyst surface, the Freundlich isotherm is an empirical model that does not provide an elementary description of the adsorption process. It is important to note that the Langmuir and Freundlich isotherms may coincide at moderate coverages over a wide range of pressures [56]. In this case, it can be assumed that the heat of adsorption is independent of the coverage, and the surface heterogeneity is negligible [56]. In other words, the surface behaves as an ideal surface. While the Ni-H-Beta used in the present study was a real surface with dissimilar active sites (nickel and residual Brønsted sites), one may assume that the individual site domains (domains where the sites are equal) behaved as uniform surfaces—the same assumption proposed by Langmuir—so that both the Langmuir and Freundlich isotherms may be used to model the experimental adsorption data. In this study, we compared the quality of the fitting of Langmuir and Freundlich isotherms to assess the extent of site heterogeneity on the catalyst surface.

Table 1 lists the Langmuir isotherms developed in the present work for ethylene coverage on the Ni-H-Beta catalyst. All the isotherms were based on *Mechanisms A, B, and C* depicted in Figure 1, except for the additional model that involved ethylene adsorption over two sites (model not depicted in Figure 1). The Langmuir isotherm expressions presented in Table 1 were used to compare the mechanism involved in the initial ethylene adsorption on the Ni-H-Beta catalyst. The main differences in these mechanisms were the number of ethylene molecules and active sites involved in the adsorption process, the nature of the nickel center formed, and the type of adsorption (simple, associative, or dissociative adsorption). In *Mechanism A* (Figure 1), ethylene dissociated over a Ni^{2+} site, forming a $[\text{Ni}(\text{II})\text{-H}]^+$ Cossee–Arlman center with an ethenyl group adsorbed. In *Mechanism B* (Figure 1), ethylene adsorbed over a $[\text{Ni}(\text{II})\text{-H}]^+$ Cossee–Arlman center that consisted of a single site formed by two individual species (one nickel and one hydride) generated “in situ” at the onset of ethylene adsorption on the catalyst. While *Mechanisms A*

and **B** involved distinct adsorption mechanisms (dissociative vs. simple), these two models produced the same Langmuir isotherm expression since they involved the adsorption of one ethylene molecule over a single site. We also considered a mechanism where ethylene adsorbed over two sites (i.e., one nickel and one Brønsted; mechanism not shown in Figure 1). The adsorption of ethylene over these sites produced a $[\text{Ni(II)-H}]^+$ species via the transfer of an electron pair from the ethylene molecule to convert H^+ into H , forming an adsorbed alkyl (i.e., ethyl). For the mechanism involving adsorption over two sites, it was assumed that ethylene underwent either simple adsorption or dissociation but could not discriminate differences in the intermediates formed via simple or dissociative adsorption. We, therefore, represented the intermediate in both cases as $[\text{Ni(II)-H}]^+ - \text{C}_2\text{H}_4$ (see Table 1). To develop the Langmuir isotherms for the mechanism involving ethylene adsorption over two sites, we assumed that the Ni^{2+} and H^+ sites were equal. This assumption was not necessarily true; however, as shown later, the catalyst surface behaved as a uniform (ideal) surface, in which all sites had the same energy. The Langmuir isotherm was also used for *Mechanism C* (Figure 1), which involved the simultaneous adsorption of two ethylene molecules over a single Ni^{2+} site.

Table 1. Langmuir isotherms developed based on the mechanisms depicted in Figure 1.

Model Description	Mechanism 1	Number of Molecules	Number of Sites	Adsorption Reaction	Langmuir Isotherm ²
Dissociation over one site	A	1	1	$\text{C}_2\text{H}_4(\text{g}) + \text{Ni}^{2+} \rightleftharpoons [\text{Ni(II)-H}]^+ - \text{C}_2\text{H}_3$	$\frac{q}{q_0} = \frac{K P_{\text{C}_2\text{H}_4}}{1 + K P_{\text{C}_2\text{H}_4}}$
Simple adsorption over one site	B	1	1	$\text{C}_2\text{H}_4(\text{g}) + [\text{Ni(II)-H}]^+ \rightleftharpoons [\text{Ni(II)-H}]^+ - \text{C}_2\text{H}_4$	
Simple adsorption over two sites	-	1	2	$\text{C}_2\text{H}_4(\text{g}) + \text{Ni}^{2+} + \text{H}^+ \rightleftharpoons [\text{Ni(II)-H}]^+ - \text{C}_2\text{H}_4$	$\frac{q}{q_0} = K P_{\text{C}_2\text{H}_4} \left(\frac{\sqrt{1+4K P_{\text{C}_2\text{H}_4}}}{2K P_{\text{C}_2\text{H}_4}} - \frac{1}{2K P_{\text{C}_2\text{H}_4}} \right)^2$
Dissociation over two sites		1	2	$\text{C}_2\text{H}_4(\text{g}) + \text{Ni}^{2+} + \text{H}^+ \rightleftharpoons [\text{Ni(II)-H}]^+ - \text{C}_2\text{H}_4$	$\frac{q}{q_0} = \frac{\sqrt{K P_{\text{C}_2\text{H}_4}}}{1 + \sqrt{K P_{\text{C}_2\text{H}_4}}}$
Association over one site	C	2	1	$2\text{C}_2\text{H}_4(\text{g}) + \text{Ni}^{2+} \rightleftharpoons \text{Ni}^{2+} - (\text{C}_2\text{H}_4)_2$	$\frac{q}{q_0} = \frac{K P_{\text{C}_2\text{H}_4}^2}{1 + K P_{\text{C}_2\text{H}_4}^2}$

¹ Mechanisms depicted in Figure 1. ² $\theta = \frac{q}{q_0}$ represents the fraction of active sites occupied by ethylene (θ ranges between 0.0 and 1.0), q expresses the moles of ethylene (moles/mg of catalyst), and q_0 represents the total adsorption capacity (in moles/mg of catalyst).

Figure 2 shows experimental ethylene adsorption isotherms on the Ni-H-Beta catalyst with 4.1 wt. % nickel at -77 and -20 °C and the fitting of the experimental data using the Freundlich isotherm (Equation (3)) and the Langmuir isotherms presented in Table 1. Values for the adjusted constants can be found in the Supporting Information (Table S1). A preliminary observation of the fitted isotherms at -77 and -20 °C showed that the Freundlich isotherm and the Langmuir isotherm that assumed the dissociation of ethylene over two sites fit the experimental data with more accuracy than the other isotherms; notably, these two isotherms produced virtually the same results. The fact that the experimental data obeyed both the Freundlich and Langmuir isotherms suggests that the heat of adsorption remained constant with ethylene coverage over the range of ethylene coverages shown in Figure 2. As a result, the catalyst was uniform under the conditions used in the adsorption study, and the extent of the site heterogeneity was small. Also, it can be assumed that intersite or adsorbate–adsorbate interactions were negligible at the surface—in other words, the adsorption sites were isolated (Ni^{2+} and H^+).

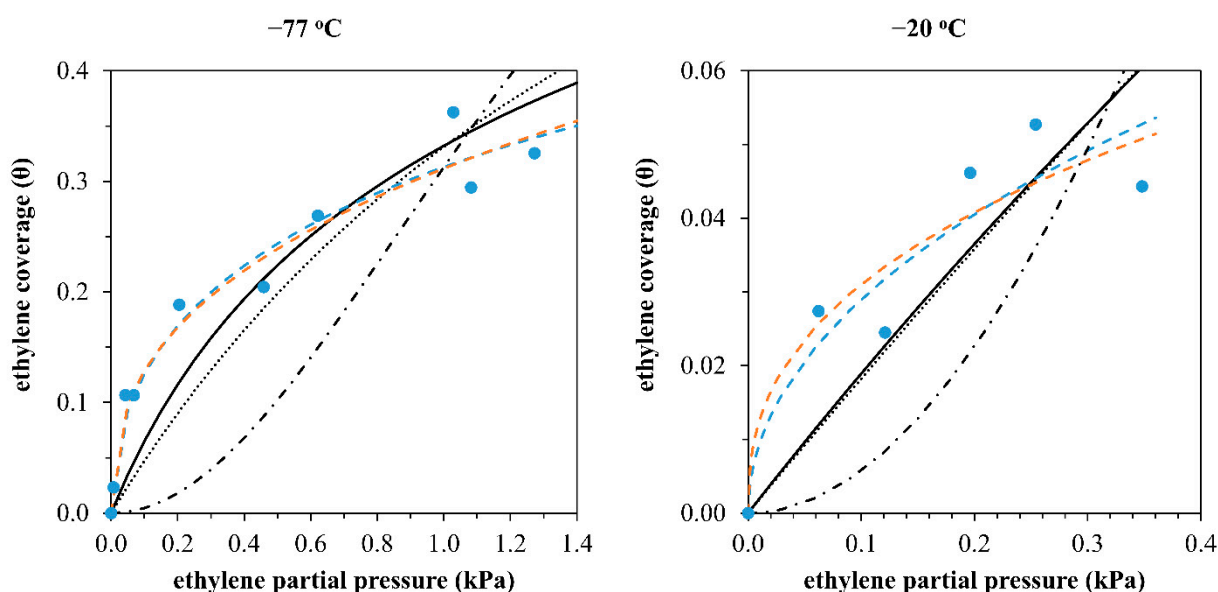


Figure 2. (●) Experimental ethylene coverage as a function of ethylene partial pressure at -77 and -20 °C. Modeled ethylene coverage (—) with the Freundlich equation and the Langmuir equations shown in Table 1: (⋯) dissociation or simple adsorption over one site, (–) simple adsorption over two sites, (–·–) dissociation over two sites, and (– – –) association over one site.

Enthalpies of adsorption of -82.8 and -68.8 kJ/mol were reported for ethylene coordination on $[\text{Ni}^{2+}\text{-ethene}]$ and $[\text{H}^+\text{-ethene}]$ sites, respectively [9]. This enthalpy difference (-14.0 kJ/mol) is less than the physisorption enthalpy of ethylene over zeolites of -22.6 kJ/mol. The hypothesis that the catalyst surface has a low extent of heterogeneity and constant heat of adsorption with ethylene coverage is consistent with the small difference in ethylene coordination enthalpy reported in the literature for nickel and Brønsted sites.

The Akaike information criterion was used to estimate the quality of the fitted Langmuir isotherms for *Mechanisms A, B, and C* and the mechanism involving adsorption over two sites relative to the experimental adsorption data. The Akaike information criterion, or *AIC*, was calculated according to the following Equation [61]:

$$AIC = 2k - n \ln(L) \quad (4)$$

where k is the number of estimated parameters, n is the number of experimental data points, and $\ln(L)$ is the maximum numerical value of the log-likelihood taken as the log of the square of the standard error (SSE). For small sample sizes, the following was used [61]:

$$AICc = AIC + \frac{2k^2 + 2k}{n - k - 1} \quad (5)$$

where *AICc* is the Akaike information criterion for small sample sizes, *AIC* is the Akaike information criterion calculated according to Equation (4), k is the number of estimated parameters, and n denotes the number of experimental data points. Equation (5) was used to compare the relative quality of the fitted models for the experimental data given in Figure 2. According to the criterion, for a given set of models, the model with the lowest *AICc* value has the highest probability of predicting a set of experimental data points. Based on the *AICc* values, the probabilities were calculated according to the following Equation [61]:

$$w_i = \frac{\exp(-0.5\Delta_i)}{\sum_{r=1}^R \exp(-0.5\Delta_r)} \quad (6)$$

where w_i is the probability that model i is more likely to predict the experimental data than the other models. Δ_i and Δ_r are the Akaike differences defined as follows [61]:

$$\Delta_{\Gamma} = AIC_{C_{\Gamma}} - AIC_{C_{minimum}} \quad (7)$$

where $AIC_{C_{\Gamma}}$ is the Akaike information criterion for a given model ($\Gamma = i$ or r), and $AIC_{C_{minimum}}$ is the minimum $AICc$ value among the set of models tested. The Akaike difference, Δ_{Γ} , can be calculated for any model. Table 2 shows the calculated AIC , $AICc$, and probabilities (w_i) according to Equations (4), (5) and (6), respectively. The comparison of the calculated probabilities in Table 2 shows that the Langmuir isotherm assuming dissociation over two active sites was 100.0% more likely to predict the experimental data than the Langmuir isotherms that assumed dissociation or simple adsorption over one site (probability = 0.0%), simple adsorption over two sites (probability = 0.0%), and association over one site (probability = 0.0%). This result indicates that the ethylene adsorption over the Ni-H-Beta catalyst obeyed a Langmuir isotherm with the dissociation of ethylene over two active sites, which were hypothesized as a nickel site and a Brønsted site.

Table 2. Statistical parameters used to compare the quality of fitting of the Langmuir adsorption isotherms presented in Table 1.

	Dissociation or Simple Adsorption over One Site	Simple Adsorption over Two Sites	Dissociation over Two Sites	Association over One Site
Mechanism	A	B	B	C
AIC	−95	−102	−124	−78
AICc	−94	−101	−123	−77
Δ	29	22	0	46
Probabilities				
	Dissociation or Simple adsorption over one site	Simple adsorption over two sites	Dissociation over two sites	Association over one site
Mechanism weight (w)	A 0.0%	B 0.0%	B 100.0%	C 0.0%

The adsorption study results partially agree with previous studies reported in the literature. The dissociation of ethylene upon adsorption on the catalyst agrees with the report from Moussa et al. [5], and the hypothesis of hydride formation during the dissociation step is consistent with the active site being $[\text{Ni(II)-H}]^+$, as reported by Joshi et al. [31,33] and postulated in our recent publication [39].

Although the experimental adsorption results presented in this publication indicated the participation of two active sites during ethylene adsorption on the catalyst—postulated as a nickel (i.e., Ni^{2+}) and an acid site (i.e., H^+)—the mechanism involved in forming nickel-hydride sites remains under debate. While Joshi et al. showed that $[\text{Ni(II)-H}]^+$ sites form in the absence of residual Brønsted sites during an induction period at the onset of ethylene adsorption on the catalyst [31] (usually at low ethylene partial pressures below 0.4 kPa), the participation of Brønsted sites during the formation of $[\text{Ni(II)-H}]^+$ centers has been postulated (based on experimental and computation evidence) by Brogaard and Olsbye [28], Brückner et al. [37], Forget et al. [29], Chen et al. [49], and Moussa et al. [5]. For example, Brogaard and Olsbye [28] proposed that a Brønsted site can form adjacent to a nickel site via the transfer of a H^+ from the ethylene molecule to the catalyst surface during ethylene adsorption over Ni^{2+} sites. This mechanism would lead to an isotherm consisting of the dissociation of ethylene over a single nickel site (similar to the activation mechanism proposed by Moussa et al. [5] shown in Figure 1, *Mechanism A*). Indeed, Moussa et al. also hypothesized the formation of H^+ sites via the dissociation of ethylene

over a Ni-H-Beta catalyst, followed by combining these sites with Ni^{2+} to form a $[\text{Ni}(\text{II})\text{-H}]^+$ Cossee–Arlman center.

The result in Figure 2 showing that the experimental adsorption data did not obey *Mechanism B* is consistent with the fact that the “in situ” formation of $[\text{Ni}(\text{II})\text{-H}]^+$ centers during a transient period at the onset of the reaction is unlikely to be probed at cryogenic temperatures; otherwise, the ethylene oligomerization on Ni zeolites conducted at temperatures of around 150 °C or above would not exhibit an induction period, as shown by Joshi et al. [31,33]. Also, while cryogenic temperatures are necessary for the adsorption study to avoid ethylene oligomerization reactions, it is possible that *Mechanisms A* and *C* are not probed at such temperatures. Nonetheless, Brogaard and Olsbye provided strong evidence that the metallacycle mechanism (*Mechanism C*) is unlikely to take place during ethylene oligomerization due to its excessively high free energy span [28]. Despite the debate regarding the mechanism proposed for the formation of the $[\text{Ni}(\text{II})\text{-H}]^+$ site, the results discussed in this section point to the participation of Brønsted sites in the formation of $[\text{Ni}(\text{II})\text{-H}]^+$ centers. However, it is also possible that at temperatures higher than -20 °C, the formation of active sites proceeds via the dissociation of ethylene over a single Ni^{2+} site (*Mechanism A*), as proposed by Moussa et al. [5], or the simple adsorption of ethylene over $[\text{Ni}(\text{II})\text{-H}]^+$ sites formed “in situ”, as proposed by Joshi et al. [31,33].

3.2. Physicochemical Properties of Ni-H-Beta Catalysts as a Function of Nickel Loading

Previous publications from our group have used the same Ni-H-Beta catalysts presented in this work (samples from the same batch) [24–27,39]. Therefore, extensive characterization, including BET, FTIR, XRD, SEM, TEM and kinetic data, is already available in the literature. We conducted further characterization via pyridine adsorption and X-ray photoelectron spectroscopy (XPS), and we reported new kinetic data for these catalysts in the present work.

Figure 3 shows infrared spectra in the pyridine region after pyridine adsorption over Ni-H-Beta catalysts with different nickel loadings. Peaks at 1450 and 1545 cm^{-1} have been assigned to pyridine coordinated with Lewis (Figure 3—LAS) and Brønsted (Figure 3—BAS) acid sites, respectively [4,5,11,62].

The introduction of nickel on the H-Beta support caused a reduction in the area of the peak assigned to BASs. The decrease in Brønsted acidity with nickel loading was corroborated by a decrease in the intensity of the peak at 1632 cm^{-1} , which was assigned to pyridinium ions (conjugated acid of pyridine). There was also a redshift of the peak at 1450 cm^{-1} with increasing nickel loading, suggesting a change in the original Lewis acidity of the H-Beta support, which was assigned to highly dispersed extra-framework aluminum [11]. These results were consistent with the replacement of some of the Brønsted sites present on the H-Beta support with cationic nickel species characterized as Lewis acids [11]. Another feature in the spectra of pyridine adsorbed on the H-Beta support was the peak centered between 1609 and 1622 cm^{-1} , which was characteristic of pyridine coordinated with extra-framework Al^{3+} . For the series of Ni-H-Beta catalysts, this peak was centered at a lower wavenumber of 1609 cm^{-1} . The peak at 1609 cm^{-1} with a prolonged shoulder at a higher wavenumber [37,63] (more visible at high nickel loadings) was assigned to pyridine coordinated with Ni^{2+} ions, indicating the presence of Ni^{2+} on the Ni-H-Beta catalysts. Similar trends have been reported in [4,11]. Therefore, the decrease in the concentration of Brønsted sites and the redshift of the peak assigned to LAS were attributed to the formation of Ni^{2+} ions in cationic exchanging positions after the impregnation of the H-Beta support with the nickel nitrate solution.

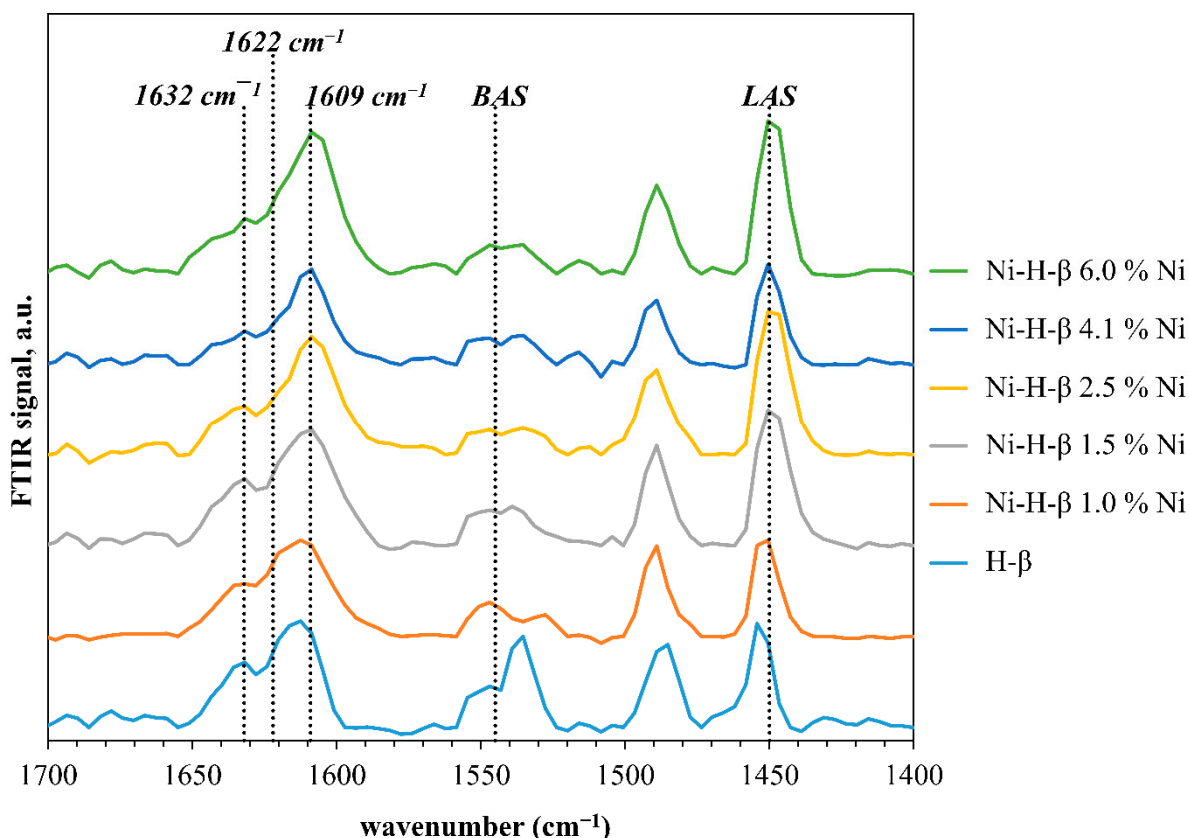


Figure 3. Infrared spectra in the pyridine region after pyridine adsorption over Ni-H-Beta catalysts with different nickel loadings followed by evacuation at 250 °C. LAS = Lewis acid site; and BAS = Brønsted acid site.

Figure 4 shows X-ray photoelectron spectra (XPS) of the Ni 2p_{3/2} region of fresh Ni-H-Beta catalysts with nickel loadings of 1.5, 2.5, and 4.1 wt. %. All the samples had characteristic peaks at 858.3 and 854.7 eV, which were assigned to highly dispersed Ni²⁺ in cationic exchanging positions and Ni²⁺ of the NiO crystals, respectively [5,64]. The absence of components at 852.0 eV—assigned to Ni⁰—demonstrated the absence or negligible quantities of zero-valent nickel on the catalyst surface [65]. We hypothesized that the formation of cationic nickel (Ni⁺ or Ni²⁺) during an induction period via the oxidative addition of Brønsted sites to Ni⁰, as previously postulated by Brückner et al. [37], was unlikely. No components at 855.5 eV were present in the XPS spectra of the fresh catalysts, suggesting the absence of Ni⁺ [5,65]. Our data indicated the presence of highly dispersed Ni²⁺ interacting with catalyst lattice oxygen and NiO crystals. While the NiO crystals may have contained nickel ions on their surfaces that promoted a small extent of oligomerization reactions [11], it is well-reported in the literature that highly dispersed Ni²⁺ ions interacting with catalyst lattice oxygen are more active. Two additional catalytic experiments were performed, one with a commercial NiO-SiO₂ catalyst (Sigma-Aldrich, product number = 675172) and another one with pure NiO nanoparticles (Sigma-Aldrich, product number = 637130), to validate the hypothesis that NiO exhibits small or negligible activity during ethylene oligomerization. In both experiments, the formation of products and consumption of ethylene was negligible, suggesting that NiO is inert during heterogeneous ethylene oligomerization.

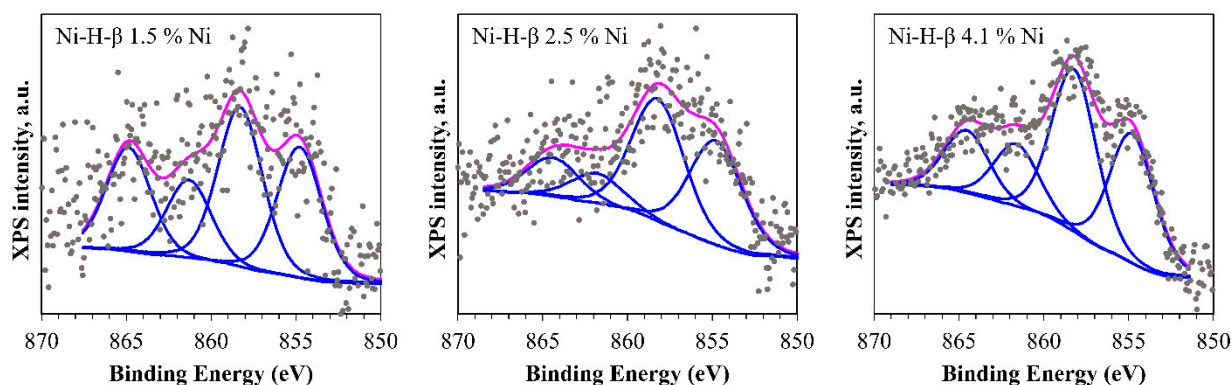


Figure 4. Ni $2p_{3/2}$ X-ray photoelectron spectra of Ni-H-Beta catalysts with nickel loadings of 1.5, 2.5, and 4.1 wt. %. Gray points: measured XPS; blue lines: fitting of individual peaks; purple line: sum of the fitted peaks.

Table 3 shows the physicochemical properties of five Ni-H-Beta catalysts with different nickel loadings. The ratio of exchanged Ni^{2+} and Ni^{2+} of the NiO ($\text{Ni}^{2+}/\text{NiO}$) were calculated using the peak areas of the XPS spectra (Figure 4), and the concentrations of LASs and BASs were calculated using the pyridine adsorption measurements (Figure 3). Table 3 also shows ethylene conversion as functions of nickel loading at 100 °C and 28 bar, the BET surface areas reported in our previous publication [27], and the relative grain size of the NiO crystals calculated according to the Scherrer equation (shown below) [66]:

$$d = \frac{K\lambda}{\beta \cos\theta} \quad (8)$$

Table 3. Physicochemical properties and ethylene conversion of Ni-H-Beta catalysts as a function of nickel loading.

Nickel Loading (wt. %)	$\frac{\text{Ni}^{2+}}{\text{NiO}}$	LAS ($\mu\text{mol/g}$)	ΔLAS	BAS	ΔLAS -BAS ($\mu\text{mol/g}$)	BET (m^2/g) ¹	Relative Grain Size of NiO Crystals (nm)	Conversion (%) ²
			(Ni^{2+})	(H^+)				
0.0	-	150	0	150	-	-	-	-
1.0	1.2	207	57	121	64	631	11	2.0
1.5	1.2	253	103	70	33	619	-	2.4
2.5	1.4	249	99	84	15	575	-	4.7
4.1	1.3	213	63	54	9	543	13	8.1
6.0	1.1	208	58	71	13	552	10	5.5
s.d. ³	-	-	-	-	-	-	-	0.2

¹ Data obtained from [27]. ² Experiments were performed at 100 °C and 28 bar. ³ Standard deviation for a triplicate at 100 °C and 28 bar.

In Equation (8), d is the relative grain size in nm, K is the shape factor, 0.94, λ is the X-ray wavelength used (1.54 Å), β is the full width at half maximum (FWHM) of the representative peak, and θ is the angular position of the peak. The peak at $2\theta = 43.2^\circ$ ((200) plane of fcc-NiO crystals) was chosen for the calculations. The XRD patterns used to obtain the FWHM were reported in our previous publication [27].

The $\text{Ni}^{2+}/\text{NiO}$ ratios in Table 3 varied between 1.1 and 1.4, with the maximum ratio at a nickel loading of 2.5 wt. %. This variation was small relative to the range of nickel loadings analyzed in this study, demonstrating that the superficial distribution of highly dispersed Ni^{2+} and NiO on the catalyst (depth less than 2 nm) was independent of the nickel loading. This analysis was consistent with the small change in the relative grain size of NiO crystals (10–13 nm) with increasing nickel loading from 1.0 to 6.0 wt. %. In Table 3,

the column denoted Δ LAS shows the difference in LAS concentrations between the series of nickel catalysts and the pristine support (Table 3, nickel loading = 0.0 wt. %). The pyridine adsorption data shows that the concentration of Δ LAS increased with increasing nickel loading, reaching a maximum of 103 $\mu\text{mol/g}$ at a nickel loading of 1.5 wt. % (Table 3, Δ LAS column). A similar trend was reported by Martinez et al. with the maximum concentration of LAS (185 $\mu\text{mol/g}$) at a nickel loading of 3.8 wt. % for a series of nickel catalysts prepared via incipient wetness impregnation [11]. The trends in Table 3 for LAS, Δ LAS, and BAS show that nickel exchanged Brønsted sites on the H-beta support and produced additional LASs with increasing nickel loading. As a result, Ni^{2+} in exchanging positions was identified as LASs, replacing acidic sites during incipient wetness impregnation.

3.3. Effect of Nickel and Brønsted Sites on Ethylene Oligomerization with Ni-H-Beta Catalysts

The results of the adsorption study suggested that ethylene adsorbs over two sites, hypothesized as Ni^{2+} and H^+ , forming a $[\text{Ni}(\text{II})\text{-H}]^+$ Cossee–Arman center. While previous reports have indicated that nickel-hydride sites may form “in situ” with the participation of Brønsted sites [28,37], our XPS results suggested that the oxidative addition of H^+ to Ni^0 is unlikely due to the absence of the latter species on the catalyst surface. Nonetheless, the results in Table 3 show a correlation between the concentration of Brønsted sites and ethylene conversion.

Table 3 shows that ethylene conversion was inversely proportional ($R^2 = 0.99$) to the difference between the concentration of LASs originating from Ni^{2+} species and the concentration of Brønsted acid sites (Table 3, $|\Delta\text{LAS} - \text{BAS}|$ column). The inversely proportional relationship between the ethylene conversion and $|\Delta\text{LAS} - \text{BAS}|$ suggested that non-coordinated Ni^{2+} and Brønsted sites reduce the probability of forming a $[\text{Ni}(\text{II})\text{-H}]^+$ active center, hindering ethylene adsorption and conversion with the Ni-H-Beta catalyst. For instance, the Ni-H-Beta catalyst with a nickel loading of 4.1 wt. % had the lowest concentration of $|\Delta\text{LAS} - \text{BAS}|$ and exhibited the maximum ethylene conversion among the catalysts tested in this work. Forget et al. [29] hypothesized that a single Brønsted acid was required close to a nickel site to form the active site for ethylene oligomerization on nickel-based solid catalysts. Hence, if a Brønsted site combines with a Ni^{2+} ion to form $[\text{Ni}(\text{II})\text{-H}]^+$, for each mole of Ni^{2+} (Δ LAS) present on the catalyst, one mole of H^+ (BAS) is consumed. As a result, the difference between the concentrations of nickel and Brønsted sites—defined in this work by the variable $|\Delta\text{LAS} - \text{BAS}|$ —expresses the amount of nickel or Brønsted sites *not involved* in the formation of nickel-hydride centers. Thus, high $|\Delta\text{LAS} - \text{BAS}|$ values were associated with high, uncoordinated site concentration and resulted in low ethylene conversion.

A clear example that uncoordinated sites reduced ethylene conversion is presented in Table 3. Even though the catalyst with a nickel loading of 1.5 wt. % had a higher concentration of coordinated $[\text{Ni}(\text{II})\text{-H}]^+$ sites (70 $\mu\text{mol/g}$) than the catalyst with a nickel loading of 4.1 wt. % (50 $\mu\text{mol/g}$), the former displayed a much lower ethylene conversion because of its much higher concentration of uncoordinated sites ($|\Delta\text{LAS} - \text{BAS}| = 33 \mu\text{mol/g}$ compared to $|\Delta\text{LAS} - \text{BAS}| = 9 \mu\text{mol/g}$ of the 4.1 wt. % nickel catalyst).

As presented in Table 1, the formation of a nickel-hydride center coupling a H^+ and a Ni^{2+} site involved the ethylene adsorption over these two sites followed by the transformation of the H^+ site into a hydride, yielding a $[\text{Ni}(\text{II})\text{-H}]^+\text{-C}_2\text{H}_4$ Cossee–Arman site, i.e., ethylene donated an electron pair ($2e^-$) of the π -bond. Figure 5 presents the mechanism of ethylene adsorption and the nature of the active center proposed in the present study. This mechanism is consistent with the results from the ethylene adsorption study, the XPS characterization of the nickel catalysts, and the pyridine adsorption experiments. While we cannot rule out the dissociation of ethylene over a single Ni^{2+} site (without the participation of a residual H^+ site) or the “in situ” formation of a $[\text{Ni}(\text{II})\text{-H}]^+$ site at higher temperatures ($> -20^\circ\text{C}$), as proposed by Moussa et al. [5] and Joshi et al., respectively, our results in Table 3 show that Brønsted sites could affect the rates of ethylene oligomerization at higher temperatures (i.e., 100°C). In addition, the results presented in this section are consistent

with the adsorption study in Section 3.1 and suggest that the uniform distribution of nickel and Brønsted species on the catalyst favored the formation of $[\text{Ni}(\text{II})\text{-H}]^+$ sites. This hypothesis is consistent with the idea that $[\text{Ni}(\text{II})\text{-H}]^+$ sites are isolated, as has been previously postulated in the literature [5,19,23,43,44]. Still, according to the mechanism depicted in Figure 5, the formation of nickel-hydride centers requires some degree of proximity between Ni^{2+} and H^+ sites, as previously indicated by Chen et al. [49].

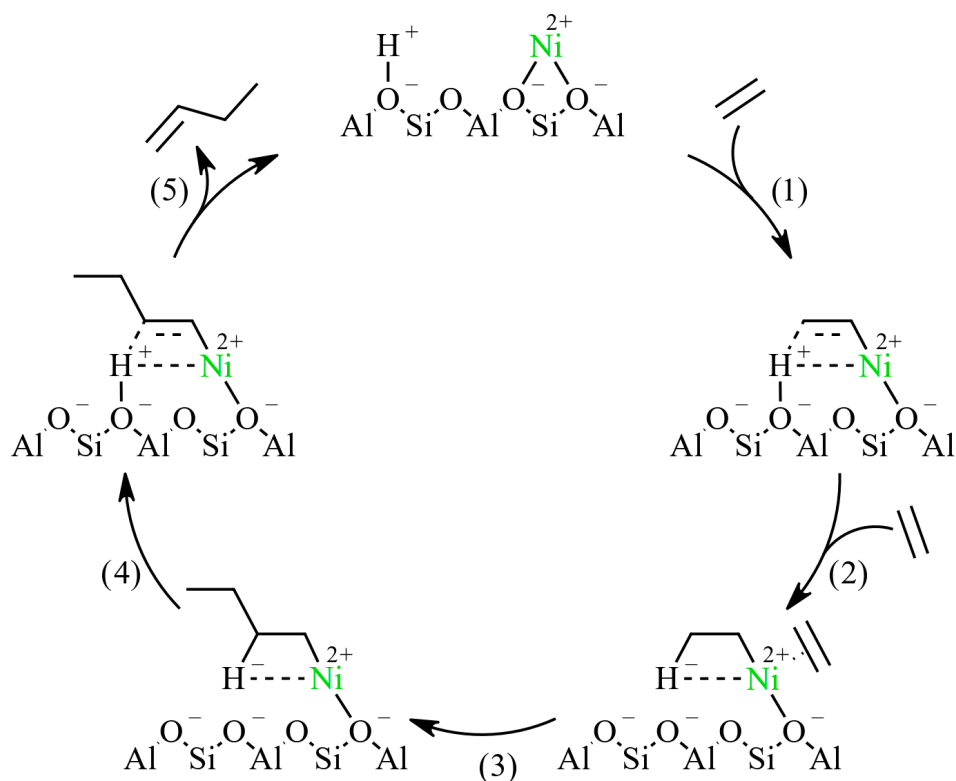


Figure 5. Proposed mechanism for formation of a nickel-hydride site involving a Brønsted acid: (1) ethylene adsorption over a Ni^{2+} site and an adjacent Brønsted site, (2) formation of $[\text{Ni}(\text{II})\text{-H}]^+$ center followed by coordination of another ethylene molecule, (3) insertion to form adsorbed butyl, (4) recovery of the Brønsted site, and (5) desorption to form a product followed by recovery of the Ni^{2+} site.

It is important to note that the ethylene oligomerization rates with catalysts containing only Brønsted sites are small under mild conditions ($T < 120\text{ }^\circ\text{C}$). According to the previous literature, such as that of Forget et al., designing nickel-based solid catalysts with high acidity is unnecessary to induce catalytic activity [29]. Hence, it is reasonable to assume that noncoordinated Brønsted sites alone exhibit small or negligible activity for primary ethylene oligomerization. Also, previous studies have investigated the contribution of acidity during ethylene oligomerization with nickel-based solid catalysts. According to these studies, ethylene consumption is proportional to the density of acid sites on the catalyst [38,67]. However, other research groups have claimed that catalyst acidity is detrimental to ethylene conversion over nickel-exchanged acidic catalysts [15–17]. They have attributed the negative effect of acid sites to the build-up of strongly adsorbed hydrocarbon chains over Brønsted sites, leading to catalyst deactivation. While the claim that Brønsted sites promote catalyst deactivation via coke build-up is true, Brønsted sites may assist in the formation of nickel-hydride centers, as hypothesized in the present work and previous works in the literature [28,37,38].

The $\text{SiO}_2/\text{Al}_2\text{O}_3$ ratio is an important parameter in the characterization of catalyst acidity, directly affecting the distribution of nickel and residual Brønsted sites on the catalyst surface. To better understand the contribution of residual Brønsted acidity on catalyst

activity, we investigated the effect of $\text{SiO}_2/\text{Al}_2\text{O}_3$ ratios on the conversion of ethylene over the Ni-H-Beta catalysts. As explained in the Experimental Method Section, H-Beta catalysts with $\text{SiO}_2/\text{Al}_2\text{O}_3$ ratios of 39 and 300 were obtained from a supplier, and three additional H-Beta catalysts with $\text{SiO}_2/\text{Al}_2\text{O}_3$ ratios of 126, 146, and 216 were produced via acid treatment of pristine H-Beta supports ($\text{SiO}_2/\text{Al}_2\text{O}_3 = 39$).

Figure 6 shows the X-ray diffraction (XRD) patterns of the pristine H-Beta supports with $\text{SiO}_2/\text{Al}_2\text{O}_3$ ratios of 39 and 300 and Ni-H-Beta catalysts with $\text{SiO}_2/\text{Al}_2\text{O}_3$ ratios of 39, 126, 146, 216, and 300 with nickel loadings of 1.0 and 2.5 wt. %. A comparison of the XRD patterns of the Ni-H-Beta catalysts and the H-Beta supports used in their preparation indicated no apparent changes in the intensity and position of the diffractions. This analysis showed that the acid treatment and nickel impregnation did not cause significant changes to the crystallographic structure of the catalysts, which is consistent with the previous literature [68].

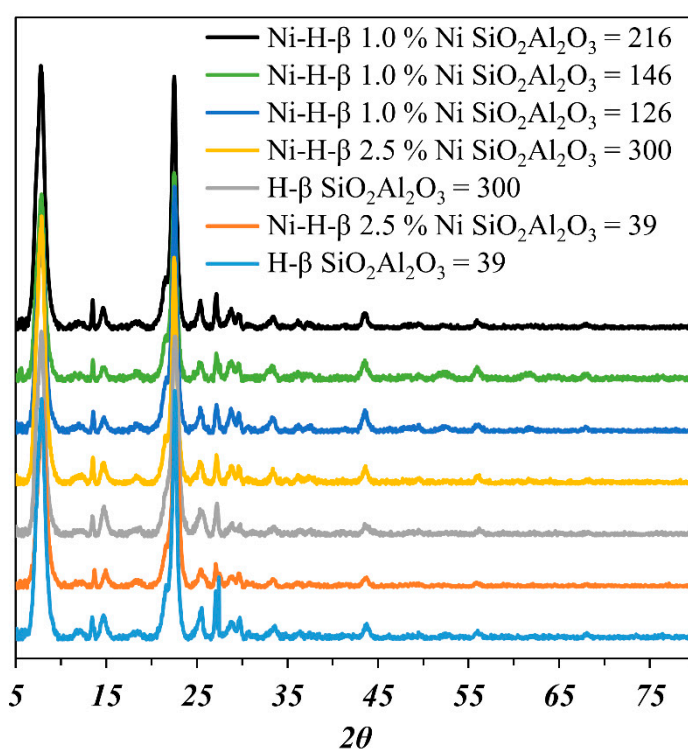


Figure 6. X-ray powder diffraction of the pristine H-Beta support and Ni-H-Beta catalysts at different $\text{SiO}_2/\text{Al}_2\text{O}_3$ ratios and nickel loadings.

Table 4 shows the concentrations of LAS, ΔLAS , BAS, and $|\Delta\text{LAS} - \text{BAS}|$ of the Ni-H-Beta catalysts with $\text{SiO}_2/\text{Al}_2\text{O}_3$ ratios of 39, 126, 146, 216, and 300 and nickel loadings of 1.0 and 2.5 wt. %, as well as the ethylene conversion and selectivity for butene (denoted as C_4), hexene (denoted as C_6), and octene (denoted as C_8) at 100 °C and 28 bar. The trends in Table 4 show that the ethylene conversion decreased with increasing $\text{SiO}_2/\text{Al}_2\text{O}_3$ ratio, in agreement with the results reported in [38,67]. At a low nickel loading (1.0 wt. %), the highest ethylene conversion was achieved for the catalyst with one of the lowest $|\Delta\text{LAS} - \text{BAS}|$ and ΔLAS concentrations. A similar trend was observed for the catalyst series with a higher nickel loading of 2.5 wt. %, with the highest ethylene conversions obtained for the Ni-H-Beta catalysts containing the lowest concentrations of noncoordinated sites of $|\Delta\text{LAS} - \text{BAS}|$. This result was consistent with our previous hypothesis that noncoordinated sites reduced the probability of forming $[\text{Ni}(\text{II})\text{-H}]^+$ Cossee–Arlman centers. Notably, the selectivity for C_4 , C_6 , and C_8 remained approximately unchanged with increasing $\text{SiO}_2/\text{Al}_2\text{O}_3$ ratios for both series of nickel catalysts. This demonstrates that the effect of noncoordinated sites was limited to decreasing the probability of forming $[\text{Ni}(\text{II})\text{-H}]^+$

Cossee–Arlman sites. Once these sites were formed, the reaction pathway and mechanism were unaffected by the catalyst's noncoordinated Ni^{2+} and H^+ sites.

Table 4. Physicochemical properties, ethylene conversion, and product selectivity of the Ni-H-Beta catalysts with different $\text{SiO}_2/\text{Al}_2\text{O}_3$ ratios and nickel loadings.

$\text{SiO}_2/\text{Al}_2\text{O}_3$	Nickel Loading (wt. %)	LAS ($\mu\text{mol/g}$)	ΔLAS ($\mu\text{mol/g}$)	BAS ($\mu\text{mol/g}$)	$ \Delta\text{LAS-BAS} $ ($\mu\text{mol/g}$)	Conversion (%) ¹	Selectivity (wt. %)		
							C_4	C_6	C_8
126	1.0	82	63	56	7	1.1	46.2	7.1	10.2
146	1.0	100	90	68	22	0.7	41.9	7.7	11.6
216	1.0	59	41	47	6	0.5	40.7	7.1	9.4
25	2.5	249	100	84	16	3.8	39.9	28.9	17.8
39	2.5	210	158	96	62	2.7	42.5	28.3	19.3
300	2.5	58	29	58	29	0.5	45.2	21.8	19.8
s.d. ²	-	-	-	-	-	0.2	6.3	3.9	0.3

¹ Data obtained at 100 °C and 28 bar. ² Standard deviation for a triplicate at 100 °C and 28 bar.

4. Conclusions

The present paper employed a series of catalyst characterization techniques combined with kinetic data to investigate the roles of nickel and Brønsted sites in ethylene oligomerization on Ni-H-Beta catalysts. Different mechanisms for ethylene oligomerization on nickel-based heterogeneous catalysts were compared via the modeling of adsorption isotherms, including the three most-accepted mechanisms (Figure 1) reported in the literature. The adsorption study results were consistent with ethylene dissociation over two active sites, hypothesized as a $[\text{Ni}(\text{II})\text{-H}]^+$ Cossee–Arlman center. X-ray photoelectron spectroscopy confirmed the presence of highly dispersed Ni^{2+} interacting with catalyst oxygen lattice, identified as LASs via pyridine adsorption. The pyridine adsorption results and the ethylene conversion over a series of Ni-H-Beta catalysts with varying nickel loadings and $\text{SiO}_2/\text{Al}_2\text{O}_3$ ratios showed that ethylene conversion was inversely proportional to the concentration of noncoordinated Ni^{2+} or H^+ , indicating that noncoordinated sites reduced the probability of forming $[\text{Ni}(\text{II})\text{-H}]^+$. Based on the experimental evidence, we hypothesized that Brønsted sites combined with Ni^{2+} to form isolated $[\text{Ni}(\text{II})\text{-H}]^+$ active centers upon ethylene adsorption over nickel-based heterogeneous catalysts. Finally, noncoordinated sites did not affect the pathway or reaction mechanism of converting ethylene with nickel-based heterogeneous catalysts.

Supplementary Materials: The following supporting information can be downloaded at: <https://www.mdpi.com/article/10.3390/catal12050565/s1>, Table S1: Adjusted constants for the models presented in Table 1.

Author Contributions: Conceptualization, G.V.S.S., F.L.P.R. and R.G.; Data curation, G.V.S.S., J.J.W.P. and P.N.T.; Formal analysis, G.V.S.S., A.D., F.L.P.R. and R.G.; Funding acquisition, F.L.P.R. and R.G.; Investigation, G.V.S.S., J.J.W.P., P.N.T., A.D., F.L.P.R. and R.G.; Methodology, G.V.S.S., A.D., F.L.P.R. and R.G.; Project administration, F.L.P.R. and R.G.; Resources, G.V.S.S., F.L.P.R. and R.G.; Supervision, A.D., F.L.P.R. and R.G.; Validation, G.V.S.S., J.J.W.P., P.N.T., F.L.P.R. and R.G.; Writing—original draft, G.V.S.S., A.D., F.L.P.R. and R.G. All authors have read and agreed to the published version of the manuscript.

Funding: This research was funded by the American Chemical Society: Petroleum Research Fund grant number 5901-ND5 and the Weyerhaeuser Endowment in Paper Science and Technology.

Data Availability Statement: Not applicable.

Acknowledgments: We acknowledge the funding provided by the American Chemical Society: Petroleum Research Fund in support of this research project (Award PRF# 5901-ND5) and the Weyerhaeuser Endowment in Paper Science and Technology. Part of this work was conducted at the Molecular Analysis Facility, a National Nanotechnology Coordinated Infrastructure site at the

University of Washington, which is supported in part by the National Science Foundation (grant NNCI-1542101), the University of Washington, the Molecular Engineering & Science Institute, and the Clean Energy Institute.

Conflicts of Interest: The authors declare no conflict of interest.

References

1. O'Connor, C.; Kojima, M. Alkene oligomerization. *Catal. Today* **1990**, *6*, 329–349. [CrossRef]
2. Finiels, A.; Fajula, F.; Hulea, V. Nickel-based solid catalysts for ethylene oligomerization—a review. *Catal. Sci. Technol.* **2014**, *4*, 2412–2426. [CrossRef]
3. McGuinness, D.S. Olefin oligomerization via metallacycles: Dimerization, trimerization, tetramerization, and beyond. *Chem. Rev.* **2011**, *111*, 2321–2341. [CrossRef] [PubMed]
4. Henry, R.; Komurcu, M.; Ganjkhanelou, Y.; Brogaard, R.Y.; Lu, L.; Jens, K.J.; Berlier, G.; Olsbye, U. Ethene oligomerization on nickel microporous and mesoporous-supported catalysts: Investigation of the active sites. *Catal. Today* **2018**, *299*, 154–163. [CrossRef]
5. Moussa, S.; Concepción, P.; Arribas, M.A.; Martínez, A. Nature of active nickel sites and initiation mechanism for ethylene oligomerization on heterogeneous Ni-beta catalysts. *ACS Catal.* **2018**, *8*, 7b03970. [CrossRef]
6. Andrei, R.D.; Popa, M.I.; Fajula, F.; Hulea, V. Heterogeneous oligomerization of ethylene over highly active and stable Ni-ALSBA-15 mesoporous catalysts. *J. Catal.* **2015**, *323*, 76–84. [CrossRef]
7. Skupińska, J. Oligomerization of α -Olefins to Higher Oligomers. *Chem. Rev.* **1991**, *91*, 613–648. [CrossRef]
8. Derouane, E.G. *Catalysts for Fine Chemical Synthesis*, 4th ed.; Derouane, E.G., Roberts, S.M., Kozhevnikov, I.V., Eds.; John Wiley & Sons, Ltd.: Hoboken, NJ, USA, 2006; ISBN 9780471490548.
9. Toch, K.; Thybaut, J.W.; Arribas, M.A.; Martínez, A.; Marin, G.B. Steering linear 1-alkene, propene or gasoline yields in ethene oligomerization via the interplay between nickel and acid sites. *Chem. Eng. Sci.* **2017**, *173*, 49–59. [CrossRef]
10. Toch, K.; Thybaut, J.W.; Marin, G.B. Ethene oligomerization on Ni-SiO₂-Al₂O₃: Experimental investigation and Single-Event MicroKinetic modeling. *Appl. Catal. A Gen.* **2015**, *489*, 292–304. [CrossRef]
11. Martínez, A.; Arribas, M.A.; Concepción, P.; Moussa, S. New bifunctional Ni-H-Beta catalysts for the heterogeneous oligomerization of ethylene. *Appl. Catal. A Gen.* **2013**, *467*, 509–518. [CrossRef]
12. Lacarriere, A.; Robin, J.; Świerczyński, D.; Finiels, A.; Fajula, F.; Luck, F.; Hulea, V. Distillate-range products from non-oil-based sources by catalytic cascade reactions. *ChemSusChem* **2012**, *5*, 1787–1792. [CrossRef] [PubMed]
13. Lallemand, M.; Finiels, A.; Fajula, F.; Hulea, V. Nature of the active sites in ethylene oligomerization catalyzed by ni-containing molecular sieves: Chemical and IR spectral investigation. *J. Phys. Chem. C* **2009**, *113*, 20360–20364. [CrossRef]
14. Lallemand, M.; Finiels, A.; Fajula, F.; Hulea, V. Continuous stirred tank reactor for ethylene oligomerization catalyzed by NiMCM-41. *Chem. Eng. J.* **2011**, *172*, 1078–1082. [CrossRef]
15. Lallemand, M.; Finiels, A.; Fajula, F.; Hulea, V. Catalytic oligomerization of ethylene over Ni-containing dealuminated Y zeolites. *Appl. Catal. A Gen.* **2006**, *301*, 196–201. [CrossRef]
16. Lallemand, M.; Rusu, O.A.; Dumitriu, E.; Finiels, A.; Fajula, F.; Hulea, V. NiMCM-36 and NiMCM-22 catalysts for the ethylene oligomerization: Effect of zeolite texture and nickel cations/acid sites ratio. *Appl. Catal. A Gen.* **2008**, *338*, 37–43. [CrossRef]
17. Hulea, V.; Fajula, F. Ni-exchanged AlMCM-41—An efficient bifunctional catalyst for ethylene oligomerization. *J. Catal.* **2004**, *225*, 213–222. [CrossRef]
18. Wang, Y.; Wang, R.; Xu, D.; Sun, C.; Ni, L.; Fu, W.; Zeng, S.; Jiang, S.; Zhang, Z.; Qiu, S. Synthesis and properties of MFI zeolites with microporous, mesoporous and macroporous hierarchical structures by a gel-casting technique. *New J. Chem.* **2016**, *40*, 4398–4405. [CrossRef]
19. Moussa, S.; Arribas, M.A.; Concepción, P.; Martínez, A. Heterogeneous oligomerization of ethylene to liquids on bifunctional Ni-based catalysts: The influence of support properties on nickel speciation and catalytic performance. *Catal. Today* **2016**, *277*, 78–88. [CrossRef]
20. Heveling, J.; Nicolaidis, C.P.; Scurrill, M.S. Identification of novel catalysts and conditions for the highly efficient and stable heterogeneous oligomerization of ethylene. *J. Chem. Soc. Chem. Commun.* **1991**, 126–127. [CrossRef]
21. Heveling, J.; Nicolaidis, C.P.; Scurrill, M.S. Catalysts and conditions for the highly efficient and stable heterogeneous oligomerization of ethylene. *Appl. Catal. A Gen.* **1998**, *173*, 1–9. [CrossRef]
22. Heydenrych, M.D.; Nicolaidis, C.P.; Scurrill, M.S. Oligomerization of ethene in a slurry reactor using a nickel(II)-exchanged silica-alumina catalyst. *J. Catal.* **2001**, *197*, 49–57. [CrossRef]
23. Hartmann, M.; Pöpl, A.; Kevan, L. Ethylene dimerization and butene isomerization in nickel-containing MCM-41 and AlMCM-41 mesoporous molecular sieves: An electron spin resonance and gas chromatography study. *J. Phys. Chem.* **1996**, *100*, 9906–9910. [CrossRef]
24. Jan, O.; Resende, F.L.P. Liquid hydrocarbon production via ethylene oligomerization over Ni-HB. *Fuel Process. Technol.* **2018**, *179*, 269–276. [CrossRef]
25. Jan, O.; Song, K.; Dichiaro, A.B.; Resende, F.L.P. Ethylene Oligomerization over Ni-H β Heterogeneous Catalysts. *Ind. Eng. Chem. Res.* **2018**, *57*, 10241–10250. [CrossRef]

26. Jan, O.; Song, K.; Dichiaro, A.; Resende, F.L.P. Oligomerization of supercritical ethylene over nickel-based silica-alumina catalysts. *Chem. Eng. Sci.* **2019**, *197*, 212–222. [[CrossRef](#)]
27. Seufitelli, G.V.S.; Resende, F.L.P. Study of the catalytic reactions of ethylene oligomerization in subcritical and supercritical media over a NiBEA catalyst. *Appl. Catal. A Gen.* **2019**, *576*, 96–107. [[CrossRef](#)]
28. Brogaard, R.Y.; Olsbye, U. Ethene Oligomerization in Ni-Containing Zeolites: Theoretical Discrimination of Reaction Mechanisms. *ACS Catal.* **2016**, *6*, 1205–1214. [[CrossRef](#)]
29. Forget, S.; Olivier-Bourbigou, H.; Delcroix, D. Homogeneous and Heterogeneous Nickel-Catalyzed Olefin Oligomerization: Experimental Investigation for a Common Mechanistic Proposition and Catalyst Optimization. *ChemCatChem* **2017**, *9*, 2408–2417. [[CrossRef](#)]
30. Metzger, E.D.; Comito, R.J.; Hendon, C.H.; Dincă, M. Mechanism of single-site molecule-like catalytic ethylene dimerization in Ni-MFU-4l. *J. Am. Chem. Soc.* **2017**, *139*, 757–762. [[CrossRef](#)]
31. Joshi, R.; Zhang, G.; Miller, J.T.; Gounder, R. Evidence for the Coordination-Insertion Mechanism of Ethene Dimerization at Nickel Cations Exchanged onto Beta Molecular Sieves. *ACS Catal.* **2018**, *8*, 11407–11422. [[CrossRef](#)]
32. Brogaard, R.Y.; Kõmurcu, M.; Dyballa, M.M.; Botan, A.; Van Speybroeck, V.; Olsbye, U.; De Wispelaere, K. Ethene Dimerization on Zeolite-Hosted Ni Ions: Reversible Mobilization of the Active Site. *ACS Catal.* **2019**, *9*, 5645–5650. [[CrossRef](#)] [[PubMed](#)]
33. Joshi, R.; Saxena, A.; Gounder, R. Mechanistic insights into alkene chain growth reactions catalyzed by nickel active sites on ordered microporous and mesoporous supports. *Catal. Sci. Technol.* **2020**, *10*, 7101–7123. [[CrossRef](#)]
34. Cossee, P. Ziegler-Natta catalysis I. Mechanism of polymerization of α -olefins with Ziegler-Natta catalysts. *J. Catal.* **1964**, *3*, 80–88. [[CrossRef](#)]
35. Arlman, E.J.; Cossee, P. Ziegler-Natta catalysis III. Stereospecific polymerization of propene with the catalyst system $\text{TiCl}_3\text{AlEt}_3$. *J. Catal.* **1964**, *3*, 99–104. [[CrossRef](#)]
36. Ehrmaier, A.; Liu, Y.; Peitz, S.; Jentys, A.; Chin, Y.H.C.; Sanchez-Sanchez, M.; Bermejo-Deval, R.; Lercher, J. Dimerization of Linear Butenes on Zeolite-Supported Ni^{2+} . *ACS Catal.* **2019**, *9*, 315–324. [[CrossRef](#)]
37. Brückner, A.; Bentrup, U.; Zanthoff, H.; Maschmeyer, D. The role of different Ni sites in supported nickel catalysts for butene dimerization under industry-like conditions. *J. Catal.* **2009**, *266*, 120–128. [[CrossRef](#)]
38. Ng, F.T.T.; Creaser, D.C. Ethylene dimerization over modified nickel exchanged Y-zeolite. *Appl. Catal. A Gen.* **1994**, *119*, 327–339. [[CrossRef](#)]
39. Seufitelli, G.V.S.; Park, J.J.W.; Tran, P.N.; Dichiaro, A.; Resende, F.L.P.; Gustafson, R. Kinetics of ethylene oligomerization over Ni-H-Beta catalysts. *J. Catal.* **2021**, *401*, 40–53. [[CrossRef](#)]
40. Escobar, M.A.; Trofymchuk, O.S.; Rodriguez, B.E.; Lopez-Lira, C.; Tapia, R.; Daniliuc, C.; Berke, H.; Nachtigall, F.M.; Santos, L.S.; Rojas, R.S. Lewis Acid Enhanced Ethene Dimerization and Alkene Isomerization-ESI-MS Identification of the Catalytically Active Pyridyldimethoxybenzimidazole Nickel(II) Hydride Species. *ACS Catal.* **2015**, *5*, 7338–7342. [[CrossRef](#)]
41. Kuhn, P.; Sémeril, D.; Matt, D.; Chetcuti, M.J.; Lutz, P. Structure–reactivity relationships in SHOP-type complexes: Tunable catalysts for the oligomerisation and polymerisation of ethylene. *J. Chem. Soc. Dalt. Trans.* **2007**, *5*, 515–528. [[CrossRef](#)]
42. Speiser, F.; Braunstein, P.; Saussine, L. Catalytic ethylene dimerization and oligomerization: Recent developments with nickel complexes containing P,N-chelating ligands. *Acc. Chem. Res.* **2005**, *38*, 784–793. [[CrossRef](#)] [[PubMed](#)]
43. Elev, I.V.; Shelimov, B.N.; Kazansky, V.B. The Role of Ni^+ Ions in the activity of NiCaY Zeolite catalysts for Ethylene Dimerization. *J. Catal.* **1984**, *89*, 470–477. [[CrossRef](#)]
44. Davydov, A.A.; Kantcheva, M.; Chepotko, M.L. FTIR spectroscopic study on nickel(II)-exchanged sulfated alumina: Nature of the active sites in the catalytic oligomerization of ethene. *Catal. Lett.* **2002**, *83*, 97–108. [[CrossRef](#)]
45. Cai, T. Studies of a new alkene oligomerization catalyst derived from nickel sulfate. *Catal. Today* **1999**, *51*, 153–160. [[CrossRef](#)]
46. Agirrezabal-Telleria, I.; Iglesia, E. Stabilization of active, selective, and regenerable Ni-based dimerization catalysts by condensation of ethene within ordered mesopores. *J. Catal.* **2017**, *352*, 505–514. [[CrossRef](#)]
47. Beucher, R.; Hulea, V.; Cammarano, C. Kinetic and mechanistic insights into Ni-ALKIT-6 catalyzed ethylene oligomerization. *React. Chem. Eng.* **2022**, *7*, 133–141. [[CrossRef](#)]
48. Jin, F.; Yan, Y.; Wu, G. Ethylene oligomerization over H- and Ni-form aluminosilicate composite with ZSM-5 and MCM-41 structure: Effect of acidity strength, nickel site, and porosity. *Catal. Today* **2020**, *355*, 148–161. [[CrossRef](#)]
49. Chen, L.; Li, G.; Wang, Z.; Li, S.; Zhang, M.; Li, X. Ethylene oligomerization over nickel supported silica-alumina catalysts with high selectivity for C10+ products. *Catalysts* **2020**, *10*, 24–30. [[CrossRef](#)]
50. Koninckx, E.; Mendes, P.S.F.; Thybaut, J.W.; Broadbelt, L.J. Ethylene oligomerization on nickel catalysts on a solid acid support: From New mechanistic insights to tunable bifunctionality. *Appl. Catal. A Gen.* **2021**, *624*, 118296. [[CrossRef](#)]
51. Emeis, C.A. Determination of Integrated Molar Extinction Coefficients for Infrared Absorption Bands of Pyridine Adsorbed on Solid Acid Catalysts. *J. Catal.* **1993**, *141*, 347–354. [[CrossRef](#)]
52. Langmuir, I. The adsorption of gases on plane surfaces of glass, mica and platinum. *J. Am. Chem. Soc.* **1918**, *40*, 1361–1403. [[CrossRef](#)]
53. Vannice, M.A. Modeling Reactions on Uniform (Ideal) Surfaces. In *Kinetics of Catalytic Reactions*; Springer: Boston, MA, USA, 2005; pp. 141–207.
54. Foo, K.Y.; Hameed, B.H. Insights into the modeling of adsorption isotherm systems. *Chem. Eng. J. J.* **2010**, *156*, 2–10. [[CrossRef](#)]

55. Choudhary, V.R.; Mayadevi, S. Sorption Isotherms of Methane, Ethane, Ethylene, and Carbon Dioxide on ALPO-5 and SAPO-5. *Langmuir* **1996**, *12*, 980–986. [[CrossRef](#)]
56. Hayward, D.O.; Trapnell, B. *Chemisorption*; Butterworths: London, UK, 1964.
57. Rideal, E.K. *Surface Chemistry*; Cambridge England University Press: Cambridge, UK, 1930.
58. Zeldowitsch, J. Adsorption site energy distribution. *Acta Phys. Chim. URSS* **1934**, *1.1*, 961–973.
59. Halsey, G.; Taylor, H.S. The Adsorption of Hydrogen on Tungsten Powders. *J. Chem. Phys.* **1947**, *15*, 624–630. [[CrossRef](#)]
60. Halsey, G.D. The Role of Surface Heterogeneity in Adsorption. *Adv. Cata.* **1952**, *4*, 259–269.
61. Burnham, K.P.; Anderson, D.R. *Model Selection and Inference: A Practical Information-Theoretic Approach*, 2nd ed.; Springer: New York, NY, USA, 2002; ISBN 0387953647.
62. Lee, M.; Yoon, J.W.; Kim, Y.; Yoon, J.S.; Chae, H.J.; Han, Y.H.; Hwang, D.W. Ni/SIRAL-30 as a heterogeneous catalyst for ethylene oligomerization. *Appl. Catal. A Gen.* **2018**, *562*, 87–93. [[CrossRef](#)]
63. Vázquez, M.I.; Corma, A.; Fornés, V. Characterization of NiO supported on zeolite Y, by pyridine adsorption. *Zeolites* **1986**, *6*, 271–274. [[CrossRef](#)]
64. Baran, R.; Kamińska, I.I.; Śrębowata, A.; Dzwigaj, S. Selective hydrodechlorination of 1,2-dichloroethane on NiSiBEA zeolite catalyst: Influence of the preparation procedure on a high dispersion of Ni centers. *Microporous Mesoporous Mater.* **2013**, *169*, 120–127. [[CrossRef](#)]
65. Domnick, R.; Held, G.; Witte, P.; Steinrück, H.P. The transition from oxygen chemisorption to oxidation of ultra-thin Ni layers on Cu(111). *J. Chem. Phys.* **2001**, *115*, 1902–1908. [[CrossRef](#)]
66. Scherrer, P.; Debye, P. Werk Übergeordnetes Werk. *Nachr. Ges. Wiss. Göttingen Math. physik. Klasse* **1918**, *2*, 101–120.
67. Espinoza, R.L.; Nicolaidis, C.P.; Korf, C.J.; Snel, R. Catalytic oligomerization of ethene over nickel-exchanged amorphous silica-alumina; Effect of the nickel concentration. *Appl. Catal.* **1987**, *31*, 259–266. [[CrossRef](#)]
68. Sadek, R.; Chalupka, K.A.; Mierczynski, P.; Maniukiewicz, W.; Rynkowski, J.; Gurgul, J.; Lasoń-Rydel, M.; Casale, S.; Brouri, D.; Dzwigaj, S. The catalytic performance of Ni-Co/Beta zeolite catalysts in Fischer-Tropsch synthesis. *Catalysts* **2020**, *10*, 112. [[CrossRef](#)]